

Analyst

Accepted Manuscript



This is an *Accepted Manuscript*, which has been through the Royal Society of Chemistry peer review process and has been accepted for publication.

Accepted Manuscripts are published online shortly after acceptance, before technical editing, formatting and proof reading. Using this free service, authors can make their results available to the community, in citable form, before we publish the edited article. We will replace this *Accepted Manuscript* with the edited and formatted *Advance Article* as soon as it is available.

You can find more information about *Accepted Manuscripts* in the [Information for Authors](#).

Please note that technical editing may introduce minor changes to the text and/or graphics, which may alter content. The journal's standard [Terms & Conditions](#) and the [Ethical guidelines](#) still apply. In no event shall the Royal Society of Chemistry be held responsible for any errors or omissions in this *Accepted Manuscript* or any consequences arising from the use of any information it contains.

1
2
3
4 **Reconstructing accurate ToF-SIMS depth profiles for organic materials with**
5 **differential sputter rates**
6
7
8

9
10 Adam J. Taylor ^{a, b}

11 Daniel J. Graham ^{a, c}

12
13 David G. Castner ^{a, b, c *}
14
15

16
17 ^a National ESCA and Surface Analysis Center for Biomedical Problems (NESAC/BIO),
18 Molecular Engineering and Sciences Institute, University of Washington, Seattle, WA,
19 USA.
20
21

22 ^b Department of Chemical Engineering, University of Washington, Seattle, WA, USA.
23

24 ^c Department of Bioengineering, University of Washington, Seattle, WA, USA.
25
26

27
28 * corresponding author: castner@uw.edu. +1 206-543-8094.
29
30
31
32
33
34
35
36
37
38
39
40
41
42
43
44
45
46
47
48
49
50
51
52
53
54
55
56
57
58
59
60

Abstract

To properly process and reconstruct 3D ToF-SIMS data from systems such as multi-component polymers, drug delivery scaffolds, cells and tissues, it is important to understand the sputtering behavior of the sample. Modern cluster sources enable efficient and stable sputtering of many organics materials. However, not all materials sputter at the same rate and few studies have explored how different sputter rates may distort reconstructed depth profiles of multicomponent materials. In this study spun-cast bilayer polymer films of polystyrene and PMMA are used as model systems to optimize methods for the reconstruction of depth profiles in systems exhibiting different sputter rates between components. Transforming the bilayer depth profile from sputter time to depth using a single sputter rate fails to account for sputter rate variations during the profile. This leads to inaccurate apparent layer thicknesses and interfacial positions, as well as the appearance of continued sputtering into the substrate. Applying measured single component sputter rates to the bilayer films with a step change in sputter rate at the interfaces yields more accurate film thickness and interface positions. The transformation can be further improved by applying a linear sputter rate transition across the interface, thus modeling the sputter rate changes seen in polymer blends. This more closely reflects the expected sputtering behavior. This study highlights the need for both accurate evaluation of component sputter rates and the careful conversion of sputter time to depth, if accurate 3D reconstructions of complex multi-component organic and biological samples are to be achieved. The effects of errors in sputter rate determination are also explored.

Introduction

The capability of argon gas cluster ion beam (GCIB) sources to effectively sputter organic materials with minimal surface damage has expanded the range of systems that may be studied by ToF-SIMS sputter depth profiling and 3D imaging. These include multicomponent organic systems that form key components of diverse technologies including organic photovoltaics¹ drug eluting stents^{2,3} and model polymeric multilayer systems^{4,5}. Argon cluster sources have proved similarly valuable for the analysis of biological materials such as amino acids⁶, lipids⁷ and peptides⁸. Analysis by ToF-SIMS has the potential to provide useful information about the composition, dimensions and spatial locations of features, interfaces and defects in such systems. However, answering questions about these systems requires accurate calibration and scaling along the z-axis (depth) during analysis of depth profiles and 3D images. When a uniform sputter rate through the sample, including the substrate, may be assumed, depth profile calibration can be performed by simply calculating a single sputter rate based on the time to sputter to the location of a known feature. The location of other features and interfaces can then be inferred directly from the sputter time required to reach the area of interest. However, many organic materials sputter at different rates^{9,10}. Such differences in sputtering may introduce a number of artifacts, which require careful consideration during data reconstruction. These include the distortion of apparent feature dimensions and spatial locations. These artifacts become more pronounced as the difference in sputter rates increases.

The analysis and reconstruction of depth profiles has been of interest to researchers using both XPS and SIMS. Of particular interest is the ability to determine interface and delta layer positions within multilayer or mixed systems¹¹⁻¹⁴. Several studies have described the need for, and methods of, correcting for a number of depth profiling artifacts. These include changing sputter rates in highly topographic samples¹⁵, and beam-damage induced sputter rate deterioration^{16,17}. However, few studies have used methods to identify and correct for different component sputter rates^{18,19}. In some cases differences in sputter rates may be minimized through careful selection of cluster size

1
2
3 and energy⁹. However, this may not provide sufficient range of sputter-rate
4 manipulation. Approaches to dynamically measure sputter yield, through a quartz crystal
5 microbalance¹⁰ or secondary neutral mass spectrometry²⁰, have been proposed. More
6 simply, correction for different sputter rates can be applied during depth calibration
7 using component sputter rates calculated from single-component films. This study
8 demonstrates the application and value of such post-hoc correction in a spun-cast
9 polystyrene-PMMA bilayer system. This polymer pairing was selected due to its
10 previously demonstrated differences in sputter rate⁹.
11
12
13
14
15
16
17

18
19 In this study we demonstrate that (1) when differences in sputter rates between
20 components are not taken into account reconstructed depth profiles are inaccurate; (2)
21 application of individual component sputter rates allows for accurate depth profiles to be
22 transformed from sputter time/dose to depth; (3) accounting for the transition between
23 different sputter rates across an interface may further improve profile reconstruction;
24 and (4) that small deviations in sputter rate determination can have significant effects on
25 the reconstructed depth profile.
26
27
28
29
30
31
32
33
34
35
36
37
38
39
40
41
42
43
44
45
46
47
48
49
50
51
52
53
54
55
56
57
58
59
60

Results and discussion

Characterization of single-component and bilayer films

Thin polymer films of polystyrene and PMMA, and bilayers of polystyrene on PMMA, were prepared by spin-casting from selective solvents. XPS analysis of single-component and bilayer films was performed to validate composition of single component films and assess continuity of the polystyrene overlayer in bilayer films. XPS spectra and calculated atomic percentages for both polystyrene and PMMA are in agreement with those previously reported for these materials²¹⁻²⁴. Table 1A shows atomic percentages of carbon and oxygen derived from XPS survey spectra. Atomic percentages of carbon and oxygen in single component films are in agreement with the expected stoichiometry. Figure 1 shows XPS high resolution C1s scans from representative PMMA, polystyrene, and bilayer films. In the C1s region, polystyrene exhibits a single peak at 285 eV, representing the C-H bond and a small peak near 292 eV representing the π - π^* shakeup characteristic of the π bonds in the aromatic ring. PMMA exhibits a more complex C1s peak with peaks at 285 eV (C-C/C-H), 286.6 eV (C-O-C) and 288.8 eV (O-C=O). These regions are quantified in table 1B. The C1s region for the bilayer sample appears identical to those for pure polystyrene, with a single peak at 285 eV and a π - π^* shakeup peak near 292 eV. Additionally the atom percentage of oxygen in the bilayer films is <1%. This suggests that the polystyrene forms an intact overlayer, providing complete coverage of the underlying PMMA. This is in line with previous reports detailing selection of 1-chloropentane as an optimal solvent for directly spin casting polystyrene overlayers on PMMA²⁵.

Determination of sputter rates

To define an accurate sputter rate, the sputter time or dose through a known thickness of material is required. Table 2 shows measured film thicknesses and sputter times to the polymer-substrate interface, along with the calculated sputter rates, for single component polystyrene and PMMA films. Thicknesses of single component and bilayer films were measured by AFM profiling of a trench cut in the film by a scalpel blade. AFM

1
2
3 was chosen as it allows direct measurement of film thickness. Polystyrene single
4 component films have a mean thickness of $114 \text{ nm} \pm 7 \text{ nm}$ (mean \pm SD) and are slightly
5 thicker than the PMMA single component films, which have a mean thickness of 105 ± 9
6 nm. Within experimental error, the sum of single component film thicknesses (220 nm)
7 is not significantly different from the measured bilayer film thickness (223 nm),
8 suggesting minimal interfacial mixing prior to depth profiling.
9

10
11 From single-component films we see that PMMA sputters 1.97 times faster than
12 polystyrene with sputter rates of 4.69 nm/s (PMMA) and 2.37 nm/s (polystyrene),
13 respectively. These sputter rates may be converted to sputter yields of $0.108 \text{ nm}^3/\text{atom}$
14 (PMMA) and $0.055 \text{ nm}^3/\text{atom}$ (polystyrene) respectively, which are closely comparable
15 to literature reported yields for argon clusters of same energy per atom²⁶⁻²⁸. The
16 difference between polystyrene and PMMA sputter rates compares favorably with
17 reported sputter yields for the same polymers, using argon clusters of same energy per
18 atom, in which the sputter yield of PMMA is 2.2 times that of polystyrene⁹. It is important
19 to note that the way in which sputtering rate decreases with sputter ion energy will vary
20 between materials and is a function of variables including primary ion beam type, cluster
21 size and energy^{9,10,27,29}.
22
23
24
25
26
27
28
29
30
31
32
33
34
35

36 **Depth profile of representative bilayer**

37
38
39 Figure 2A shows a representative ToF-SIMS depth profile through a polystyrene-PMMA
40 bilayer. The intensities of characteristic ions for each layer (Polystyrene: C_7H_7^+ , m/z 91;
41 PMMA: $\text{C}_4\text{H}_5\text{O}^+$, m/z 69; Silicon: Si^+ , m/z 28) are plotted on a \log_{10} scale against sputter
42 time. Within the initial polystyrene layer the intensity of C_7H_7^+ is stable. Between
43 approximately 45 and 55 seconds of sputtering time the intensity of C_7H_7^+ falls while
44 that of $\text{C}_4\text{H}_5\text{O}^+$ rises as the profile crosses the polystyrene-PMMA interface. In the
45 underlying PMMA layer the intensity of $\text{C}_4\text{H}_5\text{O}^+$ stabilizes. However, the intensity of
46 C_7H_7^+ does not fall to zero, but rather stabilizes at a lower intensity. This is due to the
47 fact that m/z 91.05 is a minor peak in the PMMA spectrum. Additionally a small increase
48 in the intensity of Si^+ is seen at the polystyrene-PMMA interface, likely due to
49
50
51
52
53
54
55
56
57
58
59
60

1
2
3 polydimethylsiloxane (PDMS) contamination of the PMMA stock solution. This
4 hypothesis is supported by the appearance of characteristic PDMS peaks including
5 SiC_3H_9^+ and $\text{Si}_2\text{C}_5\text{H}_{15}\text{O}^+$ in the spectra of PMMA films (data not shown). Beyond 70
6 seconds of sputter time the polymer-silicon interface is seen as a rapid drop in intensity
7 of $\text{C}_4\text{H}_5\text{O}^+$ and C_7H_7^+ , corresponding with a significant rise of the Si^+ peak. Beyond ~75
8 seconds of sputter time the Si^+ intensity stabilizes and the intensities of characteristic
9 polymer peaks continue to fall in intensity. Throughout the depth profiles, no pinholes or
10 defects were observed in ion images (data not shown), suggesting that films are intact
11 and laterally homogeneous.
12
13
14
15
16
17
18
19

20
21 In many cases it is sufficient to interpret depth profiles when plotted on their original axis
22 of sputter time or ion dose. These include systems where components sputter at similar
23 rates and where interfaces positions are tightly controlled by processing variables or
24 otherwise already known⁴. However, untransformed depth profiles only provide relative
25 information on the position of features. Since in most experimental systems the
26 locations of interfaces is not known, a translation to a depth scale is required to
27 determine their position and size. To translate to a depth scale it is necessary to
28 determine the sputter times at which polymer-polymer and polymer-substrate interfaces
29 are seen. In this study we examined the first derivative of the intensity of the
30 characteristic ion of the underlying layer ($\text{C}_4\text{H}_5\text{O}^+$ for the polystyrene-PMMA interface
31 and Si^+ for the PMMA-silicon interface) to determine interface locations. It was found
32 that identifying the position of the peak in the first derivative near an interface facilitates
33 reproducible identification of interfacial sputter times. The peak maximum of the first
34 derivative identifies the center of the interface and the full width at half maximum
35 (FWHM) the interfacial width. Table 3 shows the sputter time to the polymer-polymer
36 and polymer-substrate interfaces along with the interface widths measured using this
37 method.
38
39
40
41
42
43
44
45
46
47
48
49
50
51
52
53
54
55
56
57
58
59
60

Transformation to depth scale

Having defined interfacial positions in sputter time, it is possible to compare methods of converting sputter time to depth. Figures 2B, 2C and 2D show the results of three different transformations from sputter time to depth of the representative bilayer depth profile shown in figure 2A. The expected position of the polystyrene-PMMA and PMMA-silicon interfaces, based on measured film thickness, is marked by vertical lines (mean) and shaded areas (± 1 standard deviation). Each of the three transformation methods are discussed below.

Constant sputter rate. Figure 2B shows the resulting depth profile when a constant sputter rate is assumed. Here a constant sputter rate of 3.23 nm/s, calculated from the measured overall bilayer thickness and sputter time to polymer-silicon interface, is applied to the representative bilayer depth profile. The shape of the resulting profile is unaltered as sputter time is simply translated linearly to depth. However, where components exhibit different sputter rates this approximation may lead to incorrect conclusions regarding layer thickness and interfacial positions. In the transformed profile, three issues are noted: (1) The polystyrene-PMMA interface appears deeper than expected; (2) the polystyrene overlayer appears thicker than expected and the PMMA underlayer thinner than expected; (3) the continuation of the profile after the polymer-silicon interfaces suggests that significant sputtering into the substrate has occurred.

As the measured depth of the polymer-Si interface is used to define the constant sputter rate, this transformation places the PMMA-silicon interface at exactly at the expected interface position of 223 nm. The polystyrene-PMMA interface is predicted to be at 147 nm, 33 nm deeper than the mean measured thickness of the polystyrene film. This difference in the interface position results in significantly different relative layer thicknesses for polystyrene and PMMA than expected. If the expected interface position was not known, and different sputter rates not considered, this incorrect depth scale

1
2
3 could lead to erroneous conclusions as to the thickness of each layer and the locations
4 of the layer interfaces.
5
6

7
8 **Sputtering into silicon.** It is common for polymer depth profiling studies to be carried
9 out on inorganic substrates such as silicon, indium, titanium or gold. It is known that the
10 sputter rate of inorganic materials is orders of magnitude lower than that of organic
11 materials when using argon clusters²⁶. When depth profiles are calibrated using a single
12 depth-time measurement this can lead to the appearance of continued sputtering into
13 the substrate. In figure 2B we see that in this reconstruction yields a high Si⁺ signal
14 intensity at apparent depths ~100 nm beyond the polymer-substrate interface. While it
15 can be understood that this represents continued sampling of the silicon surface by the
16 analysis beam with little surface sputtering, and may not affect conclusions about a bulk
17 overlayer, it nevertheless is an inaccurate representation of the data. Such substrate
18 erosion artifacts are apparent in a number of studies using simple depth-time
19 transformations. These include depth profiles of HeLa Cells on silicon^{30,31} and amino
20 acid multi layers^{6,32}. In such cases an untransformed axis of sputter time, ion dose or
21 fluency may be more appropriate if the data set cannot effectively translated to length
22 units.
23
24
25
26
27
28
29
30
31
32
33
34
35

36 **Step change between component sputter rates.** In the second transformation
37 (Figure 2C) we identify each layer and assign the sputter rate determined by sputtering
38 through single polymer films. The silicon substrate was assigned a sputter rate of 0.03
39 nm/s. For this transformation we switch rates between component bulk sputter rates
40 instantaneously at the time point identified as the center of the interface (see Table 3).
41 This results in several improvements over the constant sputter rate applied previously:
42 (1) Significantly closer agreement between the predicted and expected positions of the
43 polymer-polymer and polymer-substrate interfaces; (2) predicted layer thicknesses
44 which are more closely aligned with those expected; and (3) no apparent sputtering into
45 the silicon.
46
47
48
49
50
51
52
53
54
55
56
57
58
59
60

1
2
3
4
5
6
7
8
9
10
11
12
13
14
15
16
17
18
19
20
21
22
23
24
25
26
27
28
29
30
31
32
33
34
35
36
37
38
39
40
41
42
43
44
45
46
47
48
49
50
51
52
53
54
55
56
57
58
59
60

With a step-change between sputter rates in each layer of the film, the predicted polystyrene-PMMA interface position of 113 nm is more closely in line with the expected polystyrene overlayer film thickness of 114 ± 7 nm. The predicted depth of the PMMA-silicon interface (218 nm) is within one standard deviation of the expected overall bilayer film thickness (223 ± 9 nm). This results in apparent layer thicknesses closer to that expected from the measured film thicknesses, and a more accurate profile.

Sputter rate transition across the interface. Since it is unlikely that the interface between the two polymers is absolute, we explored modeling the transition between the two polymers. This should take into account the fact that the transition between two materials often shows a rise and fall of characteristic signals as the sputtering crosses the interface versus a sharp step function. The width of, and sputtering behavior within, this region may be factors of (1) interfacial mixing during sample preparation caused by phase separation or lateral variance in interface position; (2) atomic mixing induced by ion beam damage and surface roughening during sputter or analysis cycles; (3) differences in component ionization efficiency. Each of these parameters may interact with one another.

We hypothesized that the depth profile transformation may be further improved by interpolating the transition rate across interfaces. While others have accounted for this region using the relative intensity of characteristic ions for each layer¹⁶, sputtering behavior may not follow relative ion intensity. To assess how the sputter rate transition across the polymer-polymer interface should be modeled, spun cast films of polystyrene-PMMA blends were prepared from toluene. Quantification of XPS spectra of blended polymer films (Figure 3A) shows a linear decrease in the intensity of the C1s peak (285 eV), and π - π^* shakeup peak (290 eV), and linear increase of the C=O and O1s peaks, as PMMA content is increased in polystyrene-PMMA blends, indicating that blends were well mixed. Film thicknesses of blended polymer films were measured by AFM profiling of scalpel-cut trenches. Films were depth profiled as described for single component films, and sputter rates determined relative to pure polystyrene (Figure 3B). With increasing polystyrene content an approximately linear decreasing trend in relative

1
2
3 sputter rate is observed. Therefore, to further improve the model, we allow the sputter
4 rate to change linearly between known single component sputter rates across the
5 interfacial width. In other systems it may be more appropriate to apply another function
6 to model sputter rate transition: Power-law, exponential or other functions may all be
7 easily applied. These may be applicable where a component with low sputter rate as a
8 single component exhibits a greatly enhanced sputtering in the presence of another
9 component. These effects have been observed in the sputter characteristics of some
10 drug doped polymer materials. For example, Mahoney et al. (2005) noted that pluronic-
11 P104 sputtered much more efficiently as a triblock copolymer with PLLA than as a
12 single component material³³.
13
14
15
16
17
18
19
20
21
22

Component sputter rates with linear transition Figure 2D shows the application of a
23 linear transition between component sputter rates across the width of the interfaces.
24 Pure component sputter rates are still used throughout each layer. The predicted depth
25 of the polystyrene-PMMA interface (113 nm) is seen to be comparable with that
26 predicted using a step change in sputter rates (113 nm). The linear transition between
27 sputter rates softens the shape of the interface, while moving data points slightly deeper
28 (<1 nm) than seen with the sharp transition. Here only a three data points lie in the
29 interfacial region, limiting the capability to alter profile shape during reconstruction.
30 Reconstruction of sputtering phenomena across the polymer-polymer interface would be
31 enhanced by a higher number of data points in interfacial regions.
32
33
34
35
36
37
38
39
40
41
42

The PMMA-Si interface appears at 218 nm, in line with that predicted by the step-
43 change transformation, and within one standard deviation of the expected overall bilayer
44 film thickness (223 ± 9 nm). Figure 4 shows the polymer-Si interfacial region of
45 reconstructed depth profiles in more detail. In the step-change reconstruction peak
46 intensities are seen to abruptly change at the interface. Modeling a linear transition in
47 sputter rate yields a smoother shape to the interface, and more closely reflects the
48 expected differences in sputter rate and component mixing between each sputter-
49 roughened analysis slice within the interfacial region³⁴.
50
51
52
53
54
55
56
57
58
59
60

1
2
3
4 **Consideration of phase-separation in PS-PMMA blends.** Recognizing that
5 polystyrene and PMMA are immiscible and may phase-separate, we performed AFM
6 analysis of film surfaces and sputter craters for pure polymers and a 50:50 blend. Figure
7 5A shows representative AFM height images of film surfaces before sputtering and
8 crater bases after 3, 9 or 15 seconds of sputtering. Figure 5B shows the roughness (R_q)
9 of film surfaces and crater bases, calculated from representative AFM images.
10 Horizontal line scans across representative AFM images can be found in the electronic
11 supplementary information (ESI). At the film surface, the blended film exhibits raised
12 domains ~ 250 nm across and ~ 10 nm high, indicative of phase separation-induced
13 topography. While phase separation was not promoted by an annealing step, these
14 features are of comparable scale to those previously described for polystyrene-PMMA
15 systems^{35,36}, although they may not directly correspond to chemical phase-
16 separations³⁷. Such features are not seen at the surface of either pure film, which
17 appear flat ($R_q < 1$ nm) and uniform.
18
19

20 For all films, the roughness of crater base was substantially higher than for the film
21 surface. Roughness was seen to increase with sputter time. It was seen that the
22 roughness of blended films was significantly higher than for pure films at all sputter
23 times. It was noted that the lateral feature size of the topography after sputtering was
24 smaller than the phase-separated domains seen at the film surface for the 50/50 blend.
25 These results suggest that surface features caused by polymer phase separation are
26 quickly removed by sputter-induced roughening of short lateral feature size and ~ 10 nm
27 depth range. The phase separation seen here is not expected to adversely influence
28 ToF-SIMS data interpretation, particularly given a ~ 25 -fold difference between the
29 roughness length-scale of crater bases and the SIMS analysis area. No significant
30 difference in polymer-Si interface width was observed for depth profiles of blended
31 polymers.
32
33

34 **Errors in depth profile reconstruction introduced by variability in sputter rate**
35 **determination.** Reconstructing a depth profile that is accurate and representative
36 requires confidence in the parameters used to transform the data set, in this case the
37
38
39
40
41
42
43
44
45
46
47
48
49
50
51
52
53
54
55
56
57
58
59
60

1
2
3
4
5
6
7
8
9
10
11
12
13
14
15
16
17
18
19
20
21
22
23
24
25
26
27
28
29
30
31
32
33
34
35
36
37
38
39
40
41
42
43
44
45
46
47
48
49
50
51
52
53
54
55
56
57
58
59
60

component sputter rates. Errors in component sputter rates most likely arise from errors in measuring film thicknesses and the sputter time/dose to the polymer-substrate interface since these quantities are used to calibrate the sputter rate. In this study film thickness measurements demonstrated standard deviations of 5-9 nm, approximately 5% of overall film thickness, while the standard deviation for time to polymer-Si interface in polystyrene films was 1.6 seconds (Table 2). The impact of errors in calculated sputter rates can be visualized by reconstructing depth profiles using sputter rates for polystyrene and PMMA randomly sampled from a normal distribution derived from the mean and standard deviation of calculated sputter rates (Figure 6A). For this figure, the silicon sputter rate was not modified. Significant variation in these profiles can be seen, both in polymer-polymer and polymer-Si interface position, and in relative film thickness. Within each layer, the error in sputter rate determination will linearly correlate with the resulting error in apparent layer thickness. These represent some of the errors that may be introduced to reconstructions through inaccurate sputter rate determination.

In figures 6B and 6C we highlight specific cases of erroneous reconstructions that may arise from the combination of errors in each component sputter rate. When sputter rates are sampled from the same percentile of a normal distribution derived from the mean and standard deviation of calculated sputter rates, errors are introduced both in interface position and layer thickness. Selecting sputter rates from the 5th percentile (slower sputter rate than mean) for both polystyrene and PMMA gives apparent polymer-polymer and polymer-Si interfaces shallower than for mean sputter rates. (Figure 6B). When both are selected from the 95th percentile (faster sputter rate than mean) this is reversed, with interface positions deeper than for mean sputter rates. These deviations are ± 12 nm for the polymer-polymer interface, and ± 22 nm for the polymer-silicon interface. When sputter rates from polystyrene and PMMA samples were selected from percentiles on opposite tails of their respective distribution (5th and 95th, or 95th and 5th), reconstructions place the polymer-Si interface close to that for mean values as the errors in sputter rates cancel one another out (Figure 6 C). However, they continue to displace the apparent polymer-polymer interface position by

1
2
3 up to ± 12 nm. These scenarios help visualize how errors in the determination of
4 multiple sputter rates mix to produce transformed depth profiles that may not reflect the
5 chemical distribution or thickness of the sample. These results demonstrate the
6 necessity of accurately assigning component sputter rates and validating transformed
7 profiles against expected sample thickness and interface positions. They additionally
8 highlight the potential impact of errors in their determination on reconstructed depth
9 profiles.
10
11
12
13
14
15
16

17 **Future challenges**

18
19
20 Several studies have considered depth profiling and 3D reconstruction of drug-eluting
21 polymer stents^{2,3}. In these studies depth scales were assigned using single sputter
22 rates, despite evidence of both drug-polymer phase separation and different sputter
23 rates with drug loading. This represents a scenario where consideration of differences in
24 sputtering may be advantageous. Accurate sputter rate determination is essential for
25 accurate depth profile and 3D reconstruction. In order to account for sputter rate
26 behavior within interfaces, further fundamental studies of blended materials and phase-
27 separated interfaces are required. Different sputter rates may also be expected in
28 biological materials. For sample, mammalian cells have been broadly seen to sputter at
29 the same rate across membrane, cytoplasm and nucleus^{30,38,39}, while plant tissues have
30 previously been shown to exhibit different sputter rates between cellular components⁴⁰.
31 Future studies investigating the interface of cells and polymeric scaffolds used for tissue
32 engineering will certainly require consideration of multiple sputter rates.
33
34
35
36
37
38
39
40
41
42
43
44
45

46 This study has considered the reconstruction of one-dimensional depth profiles along
47 the z-axis. Correcting for sputter rate differences in 3D ToF-SIMS is a significantly
48 greater challenge. Simple 3D corrections may in the future be accomplished by voxel-
49 stretching, however, an ideal correction would likely need to create new voxels
50 containing reconstructed spectra. Accurate depth profile reconstruction of industrially
51 and clinically relevant, multicomponent, organic and biological systems will require
52
53
54
55
56
57
58
59
60

1
2
3 careful and considered application of many factors including correction for sputter rate
4 effects addressed in this study.
5
6

7 8 **Experimental**

9 10 **Preparation of polymer films**

11 10 cm diameter silicon wafers (Silicon Valley Microelectronics, CA) were scored and
12 diced into 1 x 1 cm squares. Silicon squares were cleaned by sequential sonication in
13 ultra-pure, deionized water, dichloromethane, acetone and methanol, with two 15 min
14 washes for each solvent, and allowed to dry before use. Solutions of 30,000 MW
15 polystyrene and 15,000 MW PMMA (both Scientific Polymer Products Inc.), and 25:75,
16 50:50 or 75:25 mass ratio blends of these, were prepared by dissolving 3% wt:volume of
17 polymer in toluene (PMMA and polystyrene/PMMA blends) or 1-chloropentane (pure
18 polystyrene only) with sonication.
19
20
21
22
23
24
25
26
27

28
29 **Single component films.** Single polymer films of PMMA or polystyrene were prepared
30 by spin coating 120 μ l of polymer solution onto cleaned Si wafers at 2200 rpm for 15
31 seconds. Excess polymer solution was removed from the edge of the wafer with a
32 laboratory tissue and samples were blown dry with a nitrogen stream. Films of
33 polystyrene-PMMA blends were prepared in the same fashion.
34
35
36
37

38 **Bilayer films.** To prepare bilayer polymer films, first a PMMA film was spun cast from a
39 3% wt:vol solution in toluene on Si wafer as above. After drying overnight under vacuum
40 to ensure complete solvent evaporation, a polystyrene overlayer was spun cast from a
41 3% wt:vol solution in 1-chloropentane atop the PMMA film using the same parameters.
42
43
44
45
46

47 **Sample storage.** Samples were air dried and stored under nitrogen in tissue culture
48 polystyrene multiwell plates for less than 2 weeks until further analysis.
49
50
51

52 **Film thickness measurement.**

53 Thickness of polymer films was measured by AFM profiling. Trenches were prepared in
54 polymer films by scoring with the back of a scalpel blade. At least n=3 trenches per film
55
56
57
58
59
60

1
2
3 type were profiled using a Dimension Icon-PT AFM (Bruker). The instrument was
4 operated in ScanAsyst mode using ScanAsyst-Air tips (Bruker) with a resonant
5 frequency of 50-90 kHz and a force constant of 0.4 N/m. Height images were collected
6 across a 90 μm x 90 μm area with scan rate of 0.6 Hz and 256 samples/line. Images
7 were analyzed using NanoScope Analysis v1.5 (Bruker). Representative images (n=3)
8 were flattened using a 1st order algorithm, pre-selecting areas known to represent the
9 film surface. Trench depth was measured using the step measurement tool.
10
11
12
13
14
15
16
17

18 **Crater roughness measurement**

19
20 The roughness of sputter craters produced in spun-cast films of polystyrene, PMMA, or
21 a 50:50 blend, was determined by tapping-mode AFM. Craters measuring 600 x 600 μm
22 were produced in polymer films by sputtering using the parameters described for ToF-
23 SIMS data collection below for 3, 9 or 15 seconds. Crater bottoms and original polymer
24 surfaces were analyzed using a Dimension Icon-PT AFM (Bruker). The instrument was
25 operated in tapping mode using Tap300Al-G tips (Budget Sensors) with a resonant
26 frequency of 300 kHz and a force constant of 40 N/m. Height images were collected
27 across a 1 x 1 μm area with a scan rate of 1 Hz and 256 samples/line. Images were
28 analyzed using NanoScope Analysis v1.5 (Bruker). Representative images (n=4) were
29 flattened using a 1st order algorithm, and roughness (R_q) calculated across the whole
30 image area, excluding any notable artifacts. Horizontal line scans were reconstructed
31 from row 128 of the representative images.
32
33
34
35
36
37
38
39
40
41
42
43

44 **XPS analysis**

45
46 XPS spectra were obtained from representative bilayer and single-component and
47 blended films (n=2 for each sample) using a Kratos AXIS Ultra DLD (Kratos,
48 Manchester, UK) instrument in the “hybrid” mode (large photoelectron acceptance
49 angle) using a monochromatic Al K α X-ray source and a nominal photoelectron takeoff
50 angle 0°. Survey scans were collected between 0-1200 eV binding energy for two spots
51 per sample with an 80 eV pass energy and 1 eV step-size. High-resolution scans of the
52 C1s region were acquired with a 20 eV pass energy and 0.1 eV step-size. A low-energy
53
54
55
56
57
58
59
60

1
2
3 flood gun was used for charge neutralization. XPS data was plotted and analyzed in
4 CasaXPS v2.3 (Casa Software Ltd). All binding energies are referenced to the C1s
5 hydrocarbon peak at 285 eV.
6
7
8

9 **ToF-SIMS data collection**

10 ToF-SIMS depth profiling was performed using an ION-TOF TOF SIMS 5-100 (ION-TOF
11 GmbH, Münster, Germany) instrument equipped with a Bi_n^+ liquid metal ion gun (LMIG)
12 source and an Ar_n^+ gas cluster ion bombardment (GCIB) source. Both sources were
13 arranged with a 45° angle of incidence with respect to the substrate, and rotated 180°
14 around the z-axis with respect to each other. The analysis chamber was maintained at
15 less than 1×10^{-8} mbar. The instrument was operated in a dual-beam, non-interlaced
16 mode with sequential cycles of analysis and sputtering. 25 keV Bi_3^+ clusters were used
17 for analysis and 10 keV Ar_{1000}^+ clusters were used for sputtering. An electron flood gun
18 was used to neutralize charge build-up following sputter and analysis cycles. The target
19 current of the analysis beam was maintained at 0.05 pA. The target current of the
20 sputter source was maintained at 2.5 nA. Positive ion depth profiles were acquired using
21 a dose of 2.9×10^{11} ions/cm² per analysis cycle from a $100 \times 100 \mu\text{m}$ area at a $256 \times$
22 256 pixel density. Sputtering was carried out for 3 seconds over a $600 \times 600 \mu\text{m}$ area for
23 a dose of 1.3×10^{13} ions/cm² per sputter cycle, followed by a 0.5 second pause for
24 charge neutralization. This analysis/sputter cycle was repeated until the intensity of a
25 secondary ion characteristic of the silicon substrate (Si^+) was seen to stabilize,
26 indicating completion of depth profiling through the film. Positive secondary ion spectra
27 were mass calibrated to the CH^+ , CH_2^+ and C_2H_3^+ peaks. Mass resolution at the C_2H_3^+
28 peak (m/z 27) was typically above 6000. Peaks in the positive ion spectra at m/z 28
29 (Si^+), 69 ($\text{C}_4\text{H}_5\text{O}^+$) and 91 (C_7H_7^+), were identified as characteristic peaks of the Silicon
30 substrate, PMMA, and polystyrene respectively. Depth profile data for these peaks were
31 exported as tab separated files for plotting and transformation to a depth scale in
32 RStudio v0.98 (RStudio Inc).
33
34
35
36
37
38
39
40
41
42
43
44
45
46
47
48
49
50
51
52
53
54
55
56
57
58
59
60

Determination of interface position

The sputter time to polymer-polymer and polymer-silicon interfaces were determined from the first derivative of the \log_{10} transformed intensity of the characteristic peak of the underlying layer. The location of the maxima nearest the interface position defines the time to the interface. The width of the interface was defined as the full width at half maximum (FWHM) of this peak within the first derivative. If the peak seen in the first derivative is assumed to be Gaussian, which provides a good fit, the boundaries of the FWHM are the time points at which the intensity reaches the commonly used 16% and 84% intensity values used to characterize interfaces¹¹. This allows for semi-automated and unbiased interface determination relatively free of subjective operator errors. Both the depth profile and first derivative were fit using LOESS smoothing functions, and intensities predicted in a step-wise fashion using RStudio.

Determining component sputter rates

Component sputter rates for polystyrene and PMMA and polymer blends were calculated using single-component films. Film thicknesses measured by AFM ($n=3$) was divided by sputter time to polymer-Si interfaces determined from depth profiles ($n=3$). The average sputter rate across bilayer films was determined using the same procedure. While others have observed sputter yields up to 0.01 nm³/atom with 10 eV/atom argon clusters²⁷, we observed no resulting sputter crater from extensive sputtering of the uncoated silicon substrate. Therefore, we assumed a sputter rate of silicon as 0.03 nm/s (~ 0.001 nm³/atom at 10 eV/atom), approximately two orders of magnitude lower than that of polystyrene or PMMA, and in line with previously reported sputter rates for silicon with a C₆₀ primary ion ranging from 0.01-0.1 nm/s^{15,41}. Molecular dynamic simulations of Ar_n⁺ cluster impacts with bare silicon predict similarly low sputter yields at 10 eV/atom⁴².

Depth profile reconstruction

Plotting and depth profile transformation was performed in RStudio. Depth transformations were performed in a step-wise fashion. For step-change and linear transformations interface positions were determined as described above.

1
2
3
4
5
6
7
8
9
10
11
12
13
14
15
16
17
18
19
20
21
22
23
24
25
26
27
28
29
30
31
32
33
34
35
36
37
38
39
40
41
42
43
44
45
46
47
48
49
50
51
52
53
54
55
56
57
58
59
60

Conclusions

Many studies have investigated challenges in sputter depth profiling multicomponent systems using ToF-SIMS including depth resolution, sputter induced damage, and the ability to sputter through a wide range of materials. However, relatively few have addressed correcting for components with different sputter rates through the profile. Using spun-cast bilayer samples of polystyrene and PMMA, this study has shown the following: (1) Where the depth profile is transformed to a depth scale using a single constant sputter rate, apparent layer thicknesses do not match expected values, with the predicted polymer-polymer interface shifted ~33 nm deeper than expected (14% of total film thickness). This is due to the fact that the different sputter rates of the components were not accounted for. (2) Accounting for changes in sputter rate with a step-change between known single-component sputter rates provides layer thickness and interface positions in line with measured values. (3) Instantaneous sputter rate transition across an interface is unrealistic, and polystyrene-PMMA blends exhibit a linear increase in sputter rate with increasing PMMA content. (4) Applying a linear transition between component sputter rates across the interface width may yield a profile shape that more closely recapitulates expected sputtering phenomena when sufficient data points are collected across the interfacial width. (5) Accurate determination of sputter rates is critical to producing accurately reconstructed depth profiles. This study provides an easily implemented methodology for the translation of sputter time or ion dose to depth in depth profiles, yielding accurate interface positions and apparent layer thicknesses in scenarios where differences in sputter rates between components may otherwise provide erroneous or misleading results. It is possible that this methodology could be applied to the accurate reconstruction of 3D images of systems exhibiting differences in component sputtering behavior.

Acknowledgements

We gratefully acknowledge support of the research by NIH grant EB-002027 to NESAC/BIO, and thank Gerry Hammer for collection of XPS spectra.

References

- 1 T. Mouhib, C. Poleunis, N. Wehbe, J. J. Michels, Y. Galagan, L. Houssiau, P. Bertrand and A. Delcorte, *Analyst*, 2013, **138**, 6801–6810.
- 2 C. M. Mahoney, A. J. Fahey and A. M. Belu, *Anal Chem*, 2008, **80**, 624–632.
- 3 G. L. Fisher, A. M. Belu, C. M. Mahoney, K. Wormuth and N. Sanada, *J. Proteome Res.*, 2009, **81**, 9930–9940.
- 4 A. G. Shard, R. Havelund, M. P. Seah, S. J. Spencer, I. S. Gilmore, N. Winograd, D. Mao, T. Miyayama, E. Niehuis, D. Rading and R. Moellers, *Anal Chem*, 2012, **84**, 7865–7873.
- 5 J. Bailey, R. Havelund, P. Dubruel, A. G. Shard, I. S. Gilmore, M. R. Alexander and D. J. Scurr, *ACS Appl Mater Interfaces*, 2015, **7**, 150106143135007–2659.
- 6 N. Wehbe, T. Tabarrant, J. Brison, T. Mouhib, A. Delcorte, P. Bertrand, R. Moellers, E. Niehuis and L. Houssiau, *Surface and Interface Analysis*, 2012, **45**, 178–180.
- 7 C. Bich, R. Havelund, R. Moellers, D. Touboul, F. Kollmer, E. Niehuis, I. S. Gilmore and A. Brunelle, *J. Proteome Res.*, 2013, **85**, 7745–7752.
- 8 S. Rabbani, A. M. Barber, J. S. Fletcher, N. P. Lockyer and J. C. Vickerman, *J. Proteome Res.*, 2011, **83**, 3793–3800.
- 9 P. J. Cumpson, J. F. Portoles and N. Sano, *J. Vac. Sci. Technol. A*, 2013, **31**, 020605.
- 10 P. J. Cumpson, J. F. Portoles, A. J. Barlow and N. Sano, *J. Appl. Phys.*, 2013, **114**, 124313.
- 11 E42 Committee, *Standard Guide for Measuring Widths of Interfaces in Sputter Depth Profiling Using SIMS*, ASTM International, West Conshohocken, PA, 2011.
- 12 S. Hofmann, *Surface and Interface Analysis*, 2003, **35**, 556–563.
- 13 S. Hofmann, J. Erlewein and A. Zalar, *Thin Solid Films*, 1977, **43**, 275–283.
- 14 S. Hofmann, *J. Vac. Sci. Technol. A*, 1998, **16**, 1096.
- 15 A. Wucher, J. Cheng and N. Winograd, *Anal Chem*, 2007, **79**, 5529–5539.
- 16 M. S. Wagner, *Anal Chem*, 2004.
- 17 S. Muramoto, J. Brison and D. G. Castner, *Surface and Interface Analysis*, 2010, **43**, 58–61.
- 18 A. Wucher and H. Oechsner, *Z. Anal. Chem.*, 1989, **333**, 470–473.
- 19 A. Wucher, J. Cheng and N. Winograd, *Applied Surface Science*, 2008, **255**, 959–961.
- 20 A. Wucher and H. Oechsner, *Z. Anal. Chem.*, 1989.
- 21 W. K. Way, S. W. Rosencrance and N. Winograd, *Surface Science*, 1993.
- 22 S. W. Rosencrance, W. K. Way and N. Winograd, *Surface Science*, 1993.
- 23 A. Chilkoti, D. G. Castner and B. D. Ratner, *Appl. Spectrosc.*, AS, 1991, **45**, 209–217.
- 24 G. P. López, D. G. Castner and B. D. Ratner, *Surface and Interface Analysis*, 1991, **17**, 267–272.
- 25 D. Ennis, H. Betz and H. Ade, *J. Polym. Sci. B Polym. Phys.*, 2006, **44**, 3234–3244.
- 26 P. J. Cumpson, J. F. Portoles, A. J. Barlow, N. Sano and M. Birch, *Surface and Interface Analysis*, 2013, **45**, 1859–1868.

- 1
2
3
4
5
6
7
8
9
10
11
12
13
14
15
16
17
18
19
20
21
22
23
24
25
26
27
28
29
30
31
32
33
34
35
36
37
38
39
40
41
42
43
44
45
46
47
48
49
50
51
52
53
54
55
56
57
58
59
60
- 27 M. P. Seah, *J. Phys. Chem. C*, 2013.
- 28 V. Cristaudo, C. Poleunis, B. Czerwinski and A. Delcorte, *Surface and Interface Analysis*, 2014, **46**, 79–82.
- 29 K. Shen, A. Wucher and N. Winograd, *The Journal of Physical ...*, 2015.
- 30 J. Brison, D. S. W. Benoit, S. Muramoto, M. Robinson, P. S. Stayton and D. G. Castner, *Surface and Interface Analysis*, 2010, **43**, 354–357.
- 31 J. Brison, M. A. Robinson, D. S. W. Benoit, S. Muramoto, P. S. Stayton and D. G. Castner, *Anal Chem*, 2013, **85**, 10869–10877.
- 32 N. Wehbe, T. Mouhib, A. Delcorte, P. Bertrand, R. Moellers, E. Niehuis and L. Houssiau, *Anal Bioanal Chem*, 2014, **406**, 201–211.
- 33 C. M. Mahoney, J. Yu and J. A. Gardella, *Anal Chem*, 2005, **77**, 3570–3578.
- 34 D. Mao, A. Wucher and N. Winograd, *Anal Chem*, 2009, **82**, 57–60.
- 35 L. Kailas, J.-N. Audinot, H.-N. Migeon and P. Bertrand, *Applied Surface Science*, 2004, **231-232**, 289–295.
- 36 L. Kailas, B. Nysten and P. Bertrand, *Surface and Interface Analysis*, 2004, **36**, 1227–1230.
- 37 C. Ton-That, A. G. Shard, D. O. H. Teare and R. H. Bradley, *Polymer*, 2001, **42**, 1121–1129.
- 38 S. Chandra, W. A. Ausserer and G. H. Morrison, *J Microsc*, 1987, **148**, 223–229.
- 39 M. A. Robinson, D. J. Graham and D. G. Castner, *Anal Chem*, 2012, **84**, 4880–4885.
- 40 A. J. Patkin, S. Chandra and G. H. Morrison, *Anal Chem*, 1982, **54**, 2507–2510.
- 41 J. Cheng and N. Winograd, *Anal Chem*, 2005, **77**, 3651–3659.
- 42 N. A. Kubota, D. J. Economou and S. J. Plimpton, *J. Appl. Phys.*, 1998, **83**, 4055–4063.

1
2
3
4
5
6
7
8
9
10
11
12
13
14
15
16
17
18
19
20
21
22
23
24
25
26
27
28
29
30
31
32
33
34
35
36
37
38
39
40
41
42
43
44
45
46
47
48
49
50
51
52
53
54
55
56
57
58
59
60

Tables

A	Atom percentages from survey scan		
	PMMA	Polystyrene	Bilayer
Carbon	72.0 ± 0.8	99.1 ± 1.0	99.9 ± 0.7
Oxygen	28.0 ± 0.8	0.9 ± 1.0	0.1 ± 0.7

B	Area percentages from C1s components		
	PMMA	Polystyrene	Bilayer
C-C	54.9 ± 0.1	94.7 ± 0.6	94.7 ± 0.6
C-O	26.7 ± 0.4	NR	NR
C=O	18.4 ± 0.5	NR	NR
π - π^*	NR	5.3 ± 0.6	5.3 ± 0.6

Table 1. (A) Atomic percentages of carbon and oxygen derived from C1s and O1s regions in XPS survey spectra. (B) Area percentages for C-C, C-O-C and O-C=O components of the C1s region for PMMA, polystyrene and bilayer spun-cast polymer films. Values represent mean ± 1 standard deviation, n=3. NR represents no measured peak for that component.

Film type	Thickness, nm	Sputter time to Si interface, s	Sputter rate, nm/s	Sputter yield, nm ³ /atom
PMMA	105 ± 5	22.4 ± 0.2	4.69 ± 0.24	0.108 ± 0.006
Polystyrene	114 ± 7	48.3 ± 1.6	2.37 ± 0.16	0.055 ± 0.004
Bilayer	223 ± 9	69.0 ± 0.1	3.23 ± 0.13	0.075 ± 0.003

Table 2. Measured thicknesses and sputter times through PMMA and polystyrene films and calculated sputter rates and sputter yields. Thickness determined by AFM measurement of trench cut in film. Sputter time to Si interface determined by position of maxima of first derivative. Values represent mean ± 1 standard deviation. n=3 for both sputter time and thickness measurements, except for representative bilayer where n=2. Sputter rate calculated as thickness / time to interface.

	Transformation	PS-PMMA		PMMA-Si	
		Depth	Width	Depth	Width
Time, s	N/A	45.5	8.8	69.0	7.3
Distance, nm	Constant	147	28.5	223	23.6
	Step	113	31.6	218	17.5
	Linear	113	31.1	218	17.3

Table 3. Identified interface depths and widths from original and transformed bilayer depth profiles. Depth is determined as the position of the maxima of the first derivative of the characteristic peak of the underlying layer. Width is the FWHM local to the maxima.

		Transformation method			AFM
		Constant	Step	Linear	
Relative layer thickness	Polystyrene	66.0%	50.5%	51.7%	52.1%
	PMMA	34.0%	49.6%	48.3%	47.9

Table 4. Relative thicknesses of polystyrene and PMMA layers in bilayer film predicted using three transformation methods, compared to those expected from AFM measurement.

1
2
3
4
5
6
7
8
9
10
11
12
13
14
15
16
17
18
19
20
21
22
23
24
25
26
27
28
29
30
31
32
33
34
35
36
37
38
39
40
41
42
43
44
45
46
47
48
49
50
51
52
53
54
55
56
57
58
59
60

Figures

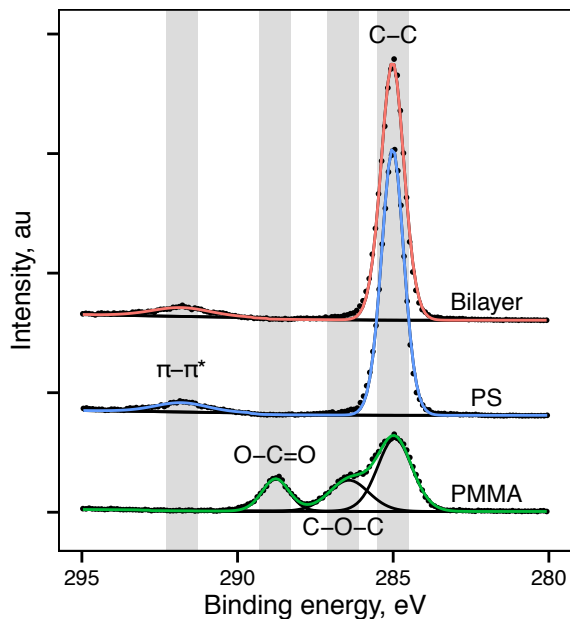


Figure 1. Representative high-resolution XPS scans of the C1s region for PMMA (bottom), polystyrene (center) and bilayer (top) spun-cast polymer films on Si wafer. Presence of the $\pi-\pi^*$ shakeup peak and absence of C-O-C and O-C=O peaks (fitted components shown in black) in bilayer sample suggests the presence of an intact polystyrene overlayer atop initially deposited PMMA film.

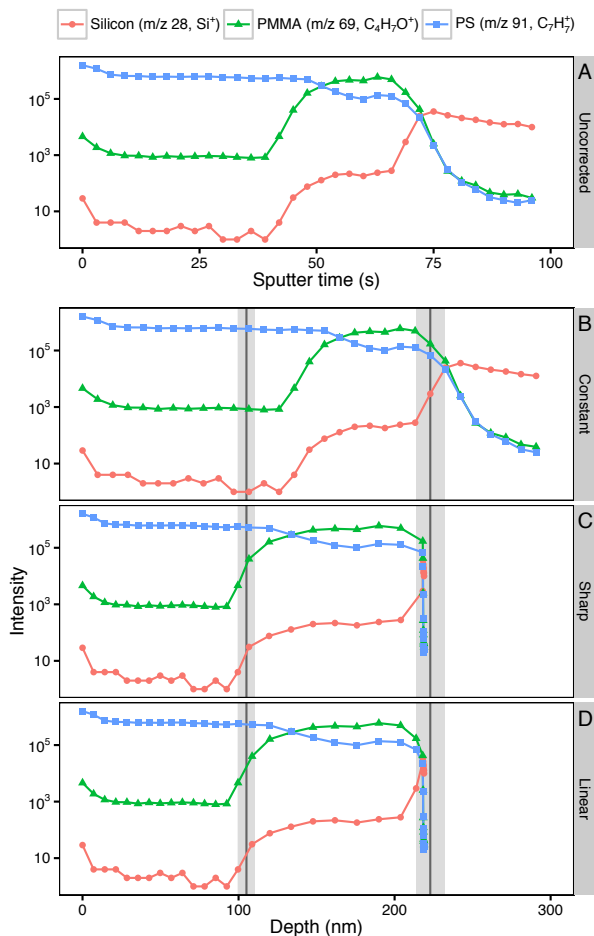


Figure 2. (A) Representative ToF-SIMS depth profile through a polystyrene-PMMA bilayer spun-cast film on Si wafer plotted against sputter time. (B-D) The same representative ToF-SIMS depth profile transformed to plot depth using different sputter rate assignment methods. (B) Transformation by constant sputter rate defined from measured bilayer thickness and sputter time to polymer-Si interface. (C) Transformation using step change between measured component sputter rates at polystyrene-PMMA and PMMA-Si interfaces. (D) Linear transition between component sputter rates across depth-resolution of polystyrene-PMMA and PMMA-Si interfaces. Intensities of characteristic peaks of each component (Silicon: Si⁺, m/z 28; PMMA: C₄H₅O⁺, m/z 69; polystyrene: C₇H₇⁺, m/z 91) are plotted on a log₁₀ intensity scale against sputter time (a) or depth from surface (b-d). Expected position of polystyrene-PMMA and PMMA-Si interfaces from AFM measurements of single-component and bilayer films are shown as vertical line (mean) and shaded area (± 1 SD).

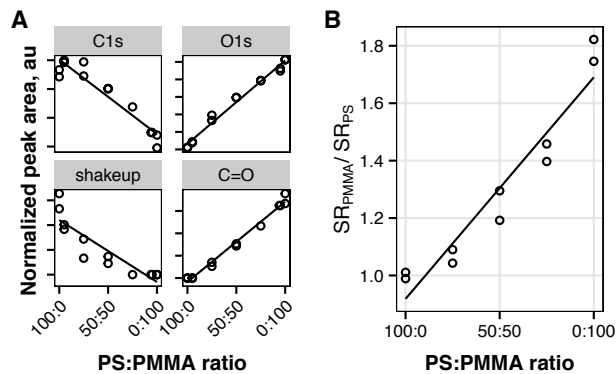


Figure 3. Characterization of polystyrene-PMMA blend films. (A) XPS peak intensities for blends. (B) Sputter rates of blends relative to pure polystyrene. Linear trend lines shown.

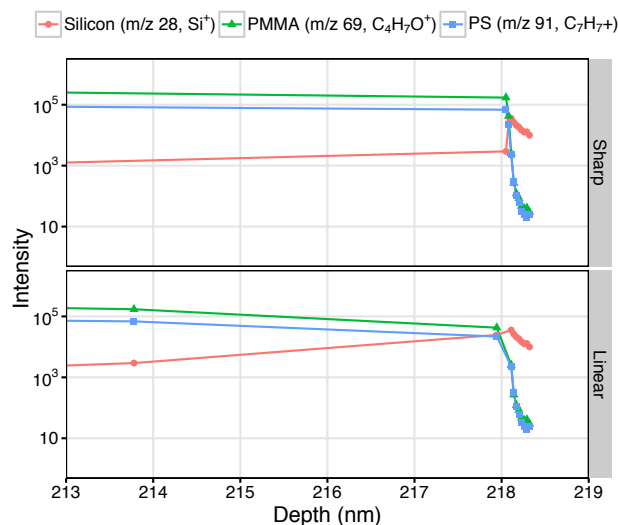


Figure 4. Enlargements from Figure 2, showing the polymer-Si interface regions of representative depth profiles reconstructed with sharp (top) and linear (bottom) sputter rate transitions. Intensities of characteristic peaks of each component (Silicon: Si⁺, m/z 28; PMMA: C₄H₅O⁺, m/z 69; polystyrene: C₇H₇⁺, m/z 91) are plotted on a log₁₀ intensity scale against depth from surface.

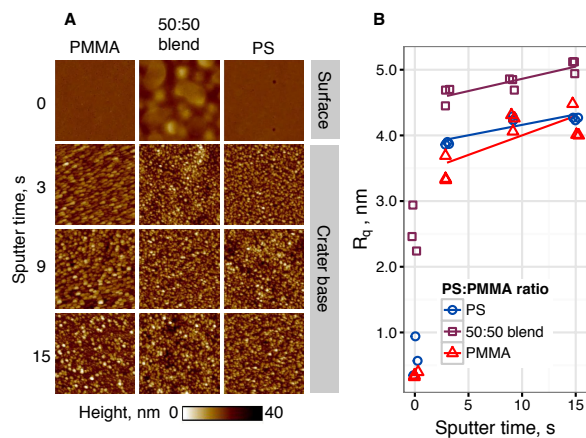


Figure 5. (A) Representative AFM height maps of PS, PMMA and blended films and crater bases after sputtering for 0 (surface), 3, 9, or 15 (crater bottom) seconds. Images show $1 \times 1 \mu\text{m}$ area. (B) Roughness parameter (R_q) of film surface and sputter crater bases in PS, PMMA and blended films. Linear trend fitted for 5-15 s of sputter time.

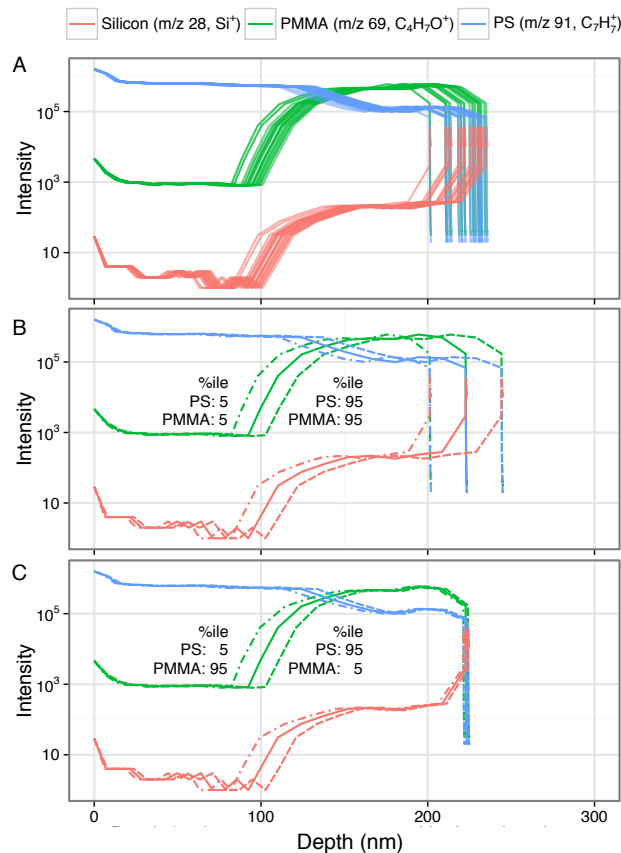


Figure 6. (A) Depth profiles ($n=20$) reconstructed from simulated sputter rates, normally distributed around the mean of the measured sputter rates. (B) Depth profiles reconstructed with sputter rates selected from the 5th (dashed line) or 95th (dot-dashed line) percentile of sputter rates for both polystyrene and PMMA. (C). Depth profiles reconstructed with sputter rates selected from the 5th and 95th percentile (dot-dashed line), or 95th and 5th percentile (dashed line) for polystyrene and PMMA respectively. Profiles reconstructed from mean sputter rates is shown with a solid line.